

Multiscale modeling of fission gas behavior in U_3Si_2 under LWR conditions

T. Barani ^{a,*}, G. Pastore ^{b,c}, D. Pizzocri ^a, D.A. Andersson ^d, C. Matthews ^d, A. Alfonsi ^b, K.A. Gamble ^b, P. Van Uffelen ^e, L. Luzzi ^a, J.D. Hales ^b

^a Politecnico di Milano, Department of Energy, Nuclear Engineering Division, via La Masa 34, I-20156 Milano, Italy

^b Idaho National Laboratory, P.O. Box 1625, Idaho Falls, ID 83415-3840, United States

^c Massachusetts Institute of Technology, Department of Nuclear Science and Engineering, 77 Massachusetts Avenue, Cambridge, MA 02139-4301, United States

^d Los Alamos National Laboratory, Materials Science and Technology Division, P.O. Box 1663, Los Alamos, NM 87545, United States

^e European Commission, Joint Research Centre, Directorate for Nuclear Safety and Security, P.O. Box 2340, 76125 Karlsruhe, Germany

ARTICLE INFO

Article history:

Received 25 January 2019

Received in revised form

10 April 2019

Accepted 24 April 2019

Available online 4 May 2019

Keywords:

Nuclear fuel modeling

Uranium silicide

Accident tolerant fuels

Fission gas behavior

Multiscale modeling

Fuel performance codes

ABSTRACT

In this work, we present a model of fission gas behavior in U_3Si_2 under light water reactor (LWR) conditions for application in engineering fuel performance codes. The model includes components for intra-granular and inter-granular behavior of fission gases. The intra-granular component is based on cluster dynamics and computes the evolution of intra-granular fission gas bubbles and swelling coupled to gas diffusion to grain boundaries. The inter-granular component describes the evolution of grain-boundary fission gas bubbles coupled to fission gas release. Given the lack of experimental data for U_3Si_2 under LWR conditions, the model is informed with parameters calculated via atomistic simulations. In particular, we derive fission gas diffusivities through density functional theory calculations, and the re-solution rate of fission gas atoms from intra-granular bubbles through binary collision approximation calculations. The developed model is applied to the simulation of an experiment for U_3Si_2 irradiated under LWR conditions available from the literature. Results point out a credible representation of fission gas swelling and release in U_3Si_2 . Finally, we perform a sensitivity analysis for the various model parameters. Based on the sensitivity analysis, indications are derived that can help in addressing future research on the characterization of the physical parameters relative to fission gas behavior in U_3Si_2 . The developed model is intended to provide a suitable infrastructure for the engineering scale calculation of fission gas behavior in U_3Si_2 that exploits a multiscale approach to fill the experimental data gap and can be progressively improved as new lower-length scale calculations and validation data become available.

© 2019 Elsevier B.V. All rights reserved.

1. Introduction

Accident tolerant fuel (ATF) systems are being considered worldwide to replace the UO_2 –zirconium system conventionally employed in light water reactors (LWRs), in order to withstand a severe accident for a considerably longer period of time than the traditional design, while preserving or improving performance under normal operating conditions [1–4]. In this context, the United States Department of Energy has accelerated research in this

area, promoting the Fuel Cycle Research and Development Advanced Fuels Campaign (AFC). The goal of the ATF program of the AFC is to guide the selection of promising fuel concepts to start a test rod irradiation in a commercial reactor by 2022.

Focusing on the nuclear fuel, uranium silicides are potential candidates to substitute uranium dioxide in LWRs. Among uranium silicides, compounds such as U_3Si , U_3Si_2 , and U_3Si_5 emerge, thanks to their interesting thermophysical properties and high uranium densities [5,6]. Those characteristics make these compounds attractive from the economic and safety point of view.

A wide experience exists worldwide in using uranium U_3Si and U_3Si_2 as fuel for research and test reactors [7–12]. On the other hand, to the best of the authors' knowledge, only one experiment

* Corresponding author.

E-mail address: tommasso.barani@polimi.it (T. Barani).

has been carried out for U_3Si_2 under power reactor conditions [13].¹

Based on the experience with research and test reactors, potential concerns about the adoption of uranium silicides in commercial reactors are related to the progressive amorphization of the crystalline structure under irradiation and high swelling rates [15–17]. In particular, amorphization of U_3Si_2 has been observed in research reactor conditions [18,19], where fuel temperatures are lower compared to LWR conditions. However, recent studies carried out on U_3Si_2 with Xe ion implantation [20–24] suggest that U_3Si_2 would remain crystalline under irradiation in LWR conditions. The polycrystalline structure of U_3Si_2 irradiated at power reactor temperatures finds confirmation in the post-irradiation metallographic images in Ref. [13].

Given the aggressive schedule, the AFC is carrying out comprehensive experiments to characterize the innovative fuel systems, as well as computational analyses to investigate the proposed materials. In this framework, given the importance of fission gas swelling and release in the thermo-mechanical performance of nuclear fuel rods, the accurate modeling of fission gas behavior as part of engineering fuel rod analysis is of the utter importance [25]. Mechanistic modeling of fission gas behavior calls for the description of complex processes, both within the fuel grains and at the grain boundaries. Intra-granular behavior involves gas bubble evolution and swelling coupled to gas atom diffusion to grain boundaries. Grain-boundary processes include precipitation, growth, and coalescence of lenticular bubbles contributing to fuel swelling, and the eventual gas venting from the grain boundaries leading to thermal fission gas release (FGR). Venting occurs after extensive gas bubble growth and interconnection, driven by gas atom and vacancy diffusion to the bubbles [25].

Rest [26] proposed a model for fission gas behavior (FGB) in U_3Si_2 , tailored for research reactor conditions, where fuel amorphization occurs. In the aforementioned work, the nucleation of fission gas bubbles was described as related to the amorphization process itself. This latter aspect constitutes a limitation to the application of the model in the analysis of U_3Si_2 in LWRs conditions. Miao et al. [27] adopted the GRASS-SST rate theory model [28], calibrating it with a combination of experimental data on U_3Si_2 from research reactors and density functional theory calculations. They studied fission gas swelling in U_3Si_2 under LWR conditions, simulating an idealized fuel rod irradiated at constant power (average linear heat rate equal to 20 kW m^{-1}) for about 3 years. Moreover, they developed a steady-state gaseous swelling correlation based on the rate theory model to be included in the BISON fuel performance code [29]. The GRASS-SST model is based on rate theory and calculates fission gas bubble size distributions considering the evolution of clusters of fission gas atoms of different sizes explicitly. While such a level of complexity provides valuable insight into the physical details, a simpler approach that only targets the average bubble size and number density may allow for a more efficient application in engineering codes, while still providing accurate calculation of the quantities of interest for the fuel rod thermo-mechanical analysis, i.e., bubble swelling and FGR.

In this work, we propose a multiscale model of fission gas swelling and release in U_3Si_2 under LWR conditions for application in engineering fuel analysis. The model includes components for intra-granular and grain-boundary behavior of fission gases. The

intra-granular component describes the evolution during irradiation of the average size and number density of intra-granular fission gas bubbles coupled to gas diffusion to grain boundaries. The grain-boundary component is based on the modeling approach originally developed for UO_2 in Ref. [30], and describes the evolution of inter-granular fission gas bubbles coupled to fission gas release from the grain boundaries to the fuel rod free volume. Experimentally derived values for important modeling parameters, such as the lattice diffusion coefficient of gas atoms and the rate of irradiation-induced re-solution of gas atoms from intra-granular bubbles, are unavailable at this time for U_3Si_2 under LWR condition. To overcome this limitation, we adopt a multiscale modeling approach (e.g. Refs. [31–34]), whereby the engineering scale model is informed with parameters extracted at the lower-length scale via atomistic simulations. In particular, we calculate the fission gas atom and point defect diffusivities through density functional theory (DFT) calculations, and the re-solution rate through binary collision approximation (BCA) calculations.

For an initial assessment of the model, we analyze the U_3Si_2 irradiation experiment from Ref. [13] and compare the results to the experimental data of gaseous swelling and fission gas release. Finally, we perform a sensitivity analysis to assess the importance of the various model parameters on the calculated fission gas swelling and release, and to derive recommendations for future research on the characterization of the physical parameters.

Extensive model validation will be performed as more substantial experimental data for U_3Si_2 under LWR conditions become available. The work is intended to provide an initial framework for the engineering analysis of fission gas behavior in U_3Si_2 that is able to exploit lower-length scale modeling for the fundamental parameters. Such a multiscale approach is particularly beneficial to accelerate progress in modeling new fuel concepts such as U_3Si_2 , for which experimental data is limited. The developed model can be progressively improved as new lower-length scale calculations and validation data become available.

The outline of the paper is as follows. In Section 2 we present the lower-length scale calculations for the derivation of model parameters. In Section 3 we describe the new engineering fission gas behavior model for U_3Si_2 . In Section 4 we apply the model to the simulation of an irradiation experiment for U_3Si_2 irradiated at temperatures compatible with LWR conditions. In Section 5 we present the sensitivity analysis. Finally, in Section 6 we draw the conclusions and discuss perspectives for this work.

2. Lower-length scale calculations

In this Section, we present the methodology and the results of the lower-length scale calculations for the derivation of the parameters used in the engineering scale model. The DFT calculations employed to derive fission gas and point defect properties in U_3Si_2 are presented in Section 2.1, while the calculation of the re-solution rate is presented in Section 2.2.

2.1. Density functional theory calculations of defects and fission gas properties

The fission gas model derived in this paper requires the diffusion rates of Xe atoms and uranium vacancies in U_3Si_2 . We rely on density functional theory calculations to provide initial estimates of these rates. The full results of the DFT calculations are presented elsewhere [35]. Here, we briefly outline the computational methodology and the key results used in the fission gas model presented in Section 3.

The approach and underlying model are the same as those described in Ref. [27], but the calculations were performed on

¹ In addition, a new experiment is underway in the framework of the ATF⁻¹ tests series of the AFC/ATF program, with two rodlets of U_3Si_2 pellets with ZIRLO[®] cladding being irradiated in the Idaho National Laboratory Advanced Test Reactor (ATR) under LWR conditions. The first non-destructive and metallography examinations demonstrated a good performance under irradiation of the U_3Si_2 fuel, at least at the low burnup (less than 20 GWd tHM^{-1}) targeted [14].

$2 \times 2 \times 3$ instead of a $2 \times 2 \times 2$ U_3Si_2 supercells and a few assumptions regarding entropies were slightly modified. The reason for increasing the size of the supercell is to improve the accuracy of, in particular, migration barriers in the **c** lattice direction of U_3Si_2 . However, none of these updates in the methodology give rise to substantial changes as compared to Ref. [27]. As an example, the predicted barriers decrease by a few tenths of an eV compared to the earlier results [27]. The DFT calculations were performed with the Vienna Ab initio Simulation Package (VASP) [36,37] and the projector augmented-wave (PAW) method for the core electrons. The exchange-correlation potential was described by the Perdew-Burke-Ernzerhof (PBE) potentials and a Hubbard U parameter was added for the uranium 5f electrons [38], which follows the same methodology as used by Noordhoek et al. [39], Middleburgh et al. [40], and Miao et al. [27]. Migration barriers were calculated using the Nudged Elastic Band method (NEB) [41]. The energy cut-off for the plane-wave expansion of the wavefunctions was set to 500 eV and sampling in reciprocal space was performed on $2 \times 2 \times 2$ Monkhorst-Pack meshes. All defect structures were fully relaxed (volume and atomic positions), while migration barriers were calculated for the volume fixed at that of the initial state.

Diffusion in U_3Si_2 is anisotropic due to its tetragonal crystal structure, which results in unique diffusion rates in the basal **a-b** plane and along the **c** axis. The migration barriers of vacancies and Xe atoms were calculated for a range of possible mechanisms, see Ref. [35] for additional details. Here we are only concerned with the fastest diffusion rate of Xe and uranium vacancies. For both of these species, the highest diffusivity is obtained for vacancy mechanisms along the **c** axis. The Xe diffusion mechanism refers to a Xe atom occupying a U 2a trap site in the U_3Si_2 crystal structure, with an assisting U 2a vacancy providing the diffusion pathway. A schematization of the aforementioned diffusion process is provided in

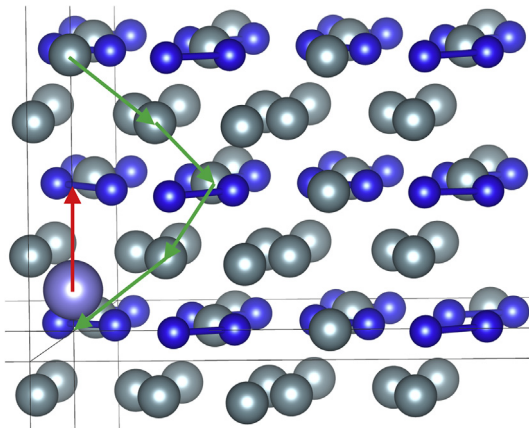


Fig. 1. Xe diffusion mechanism in U_3Si_2 involving a Xe atom in a uranium vacancy trap site and a second uranium vacancy assisting diffusion in the **c** direction. The red arrow indicates the migration step of the Xe atom, but the rate-limiting step corresponds to diffusion of the assisting uranium vacancy from one side of the cluster to the other as shown by green arrows.

Fig. 1. The rate-limiting step is given by the U 2a vacancy migrating from one side of the cluster to the other in order to initiate a new step. The intra-cluster step for the Xe atom has a much lower barrier, similar to Xe migration in UO_2 [42]. In addition to the Xe-vacancy cluster migration rate, the diffusion coefficient is a function of the relative concentration of mobile Xe clusters, which is determined by the binding energy of a U 2a vacancy to a Xe atom occupying a U 2a trap site and the concentration of U 2a vacancies in the bulk. The concentration of vacancies in bulk U_3Si_2 is estimated from the U 2a Frenkel reaction and assuming close to perfect U_3Si_2 stoichiometry, which is here assumed to imply an equal concentration of interstitials and vacancies such that the vacancy formation energy is equal to half of the U 2a Frenkel energy. It is also important to point out that the U 2a substitutional position is the most favorable trap site for Xe. The fastest uranium vacancy migration mechanism also involves a U 2a vacancy moving along the **c** axis of the U_3Si_2 crystal structure. The rate applicable to the present study is the uranium self-diffusion rate, which in addition to the vacancy migration properties also includes the concentration of vacancies obtained from the formation energy discussed above in the context of binding to the Xe trap site. These two mechanisms are assumed to provide the most relevant rates governing fission gas behavior in the present study. Note that anisotropy in diffusion may also affect these rates, however, the evaluation of this aspect is left as future work.

The defect formation and migration energies used to estimate diffusion properties are listed in Table 1.

In order to predict the actual diffusion rates, the entropies that correspond to the energies discussed above, as well as the attempt frequencies for migration, must be estimated. Those values require calculations of phonons in U_3Si_2 as well as in U_3Si_2 containing defects, which is a much more challenging and time-consuming task than the energies. For this reason, we have resorted to approximations based on experience from other materials such as UO_2 [33]. Note that these assumptions are meant to give an order of magnitude result rather than an exact value. The U 2a Frenkel entropy was set to 5 kB, the binding entropy of a vacancy to the Xe atom in U 2a trap site to 0 kB and the attempt frequency for all migration events to $5 \times 10^{12} \text{ s}^{-1}$. These values are also summarized in Table 1.

The final diffusion rates are calculated from.

$$D = \nu a^2 Z \exp(-G_a / (k_B T)) / 6 \quad (1)$$

where ν is the attempt frequency (s^{-1}), a the jump distance (m), and $Z(-)$ the number of sites available for the Xe atom or vacancy to jump to, G_a (eV) is the activation free energy given by the migration enthalpy and the defect formation and binding energies and entropies. The resulting activation energies and pre-exponential factors for diffusion are listed in Table 2.

The diffusion model above only applies to intrinsic diffusion, which implies regimes where the thermal concentration of point defects dominates over irradiation induced defects. Estimation of the latter contribution would require a combination of extensive

Table 1
The point and Xe defect properties used to estimate the diffusion rates in U_3Si_2 .

	Energy (eV)	Entropy (kB)	Attempt frequency (s^{-1})
U 2a Frenkel reaction	2.55	5	N/A
U 2a vacancy formation	1.275	2.5	N/A
U 2a migration along c axis	1.22	N/A	5×10^{12}
Binding of U 2a vacancy to Xe in a U 2a site	−0.90	0	N/A
Migration of the bound Xe–U 2a vacancy cluster	1.62	N/A	5×10^{12}

Table 2
Values adopted for the parameters of the model.

Symbol	Value or expression	Reference
D	$D_0 \exp(-\Delta H_a/kT)$ $D_0 = 5.91 \cdot 10^{-6} \text{ m}^2 \text{ s}^{-1}$ $\Delta H_a = 4.41 \cdot 10^{-19} \text{ J}$	Section 2.1 and Ref. [35]
f_n α_0	10^{-4} $2.80 \cdot 10^{-25} \left(\frac{5 \cdot 10^{-10}}{R_b} \right)^{0.23} \text{ m}^{-3}$	e.g., Veshchunov [72] Section 2.2
γ D_{ig}^v	1.16 J m^{-2} $D_{ig,0}^v \exp(-\Delta H_{a,ig}^v/kT)$ $D_{ig,0}^v = 3.35 \cdot 10^{-6} \text{ m}^2 \text{ s}^{-1}$ $\Delta H_a = 4.63 \cdot 10^{-19} \text{ J}$	Miao et al. [27,73] Section 2.1 and Ref. [35]
Ω ω	$4.09 \cdot 10^{-29} \text{ m}^3$ $8.5 \cdot 10^{-29} \text{ m}^3$	Kogai [71] —
D_{gb}^v δ_{gb} θ	$10^6 \cdot D_{ig}^v$ $5 \cdot 10^{-10} \text{ m}$ 50°	Olander and Van Uffelen [69] Kogai [71] Assumption

molecular dynamics simulations of cascades and cluster dynamics modeling. This is beyond the present scope and must be left as future work. Neglecting the contribution of irradiation-enhanced diffusion is expected to lead to an underestimation of the diffusion rates at low temperature.

2.2. Intra-granular re-resolution calculation

The re-resolution rate, or rate of fission gas knock-out from bubbles, is a key parameter for calculation of intra-granular fission gas concentrations. The balance between absorption by bubbles and knock-out leads to a pseudo steady-state concentration of mobile fission gas atoms within the grain that ultimately leads to the growth of grain-face bubbles, interconnection, and fission gas release. The full results of the calculation of re-resolution in uranium silicide will be presented elsewhere, with a brief overview of the methodology given below in order to provide a reference for the values utilized in Section 3.

The total re-resolution rate at which atoms are knocked back into the fuel can be calculated by,

$$\dot{R}(\text{s}^{-1}) = \dot{F} \int \alpha_0(R_b) n(R_b) \rho(R_b) dR_b, \quad (2)$$

where R_b is the bubble radius, F is the fission rate density, α_0 is the re-resolution parameter, n is the number of atoms in a bubble, and ρ is the bubble concentration distribution function,

$$N(\text{m}^{-3}) = \int \rho(R_b) dR_b. \quad (3)$$

Here, N is the total concentration of bubbles in the sample.

Using Equation (2), the physics of re-resolution can be distilled in a single re-resolution parameter for a given fuel type, α_0 , effectively separating environmental variables such as fission rate, temperature, and the bubble concentration distribution. The re-resolution parameter has units of knocked-out atoms per atoms in the bubble per fission, and essentially gives the probability of any given atom in a bubble to be knocked-out per fission.

The first conceptual model of fission gas re-resolution was the so-called homogeneous model presented by Nelson in 1969 [43]. The homogeneous model treats the collision of fission fragments ballistically, with gas atoms being knocked out of a gas bubble due to a collision with the fission fragments, or indirectly through a damage cascade produced by an adjacent fuel atom. In contrast to the chipping out process described by Nelson, Turnbull's model of

re-resolution published in 1971 was based on the assumption of total-destruction of the fission gas bubble by passing fission fragments [44].

The apparent conflict between the two re-resolution theories lies directly with the difference of oxide nuclear fuel; calculations by Blank and Matzke showed that the poor thermal conductivity of UO_2 results in a very large, localized thermal spike around the passing fission fragment, on the order of 2000 K [45,46]. The large temperature gradient results in a strong thermo-mechanical pulse, causing mixing of the lattice and destruction of nearby bubbles [47]. The same calculations performed for uranium carbide, which benefits from metallic-like thermal properties [45] showed a corresponding thermal spike on the order of 50 K, with effectively no resulting thermo-mechanical pulse. In light of the differences between UO_2 and UC, it is easy to see why Turnbull's theory has seen success in oxide fuels, while Nelson's theory has seen success in non-oxide fuels [48]. As a first approximation, the thermal conductivity of the fuel can be used as an indicator of the energy transfer mechanism, with poorly conducting fuels (here only UO_2) suffering from large heterogenous re-resolution, and highly conducting fuels (UC, UN, $\text{U}_3\text{Si}_{1.2,5}$) exhibiting homogenous re-resolution behavior.

Modern calculations of re-resolution have focused on UO_2 through the utilization of Molecular Dynamics (MD) simulations [49–51], but ultimately suffer from the high computational cost of MD. In light of the above discussion, re-resolution in fuels with good thermal behavior can be modeled using the homogeneous model, allowing less computationally expensive models and codes to capture the re-resolution behavior.

Recently, the Binary Collision Approximation (BCA) has been utilized to calculate the re-resolution rate in uranium carbide fuels for a wide range of bubble sizes [48]. Benefiting from the simplification of the collision kinematics to a two-body problem, the code 3DOT (3D Oregonstate TRIM) utilizes the TRIM (the Transport of Ions in Matter) algorithm [52] to capture the full cascade behavior of fission fragments interacting with fission fragments in fuel.

Utilizing the techniques provided in Matthews et al. [48], the re-resolution parameter for U_3Si_2 was calculated for a variety of different conditions such as bubble shape, surface energy, bubble radius, and temperature. Beyond a general decrease in α_0 as a function of radius, many of the parameters that go into the BCA calculations result in minimal deviation in the re-resolution parameter α_0 . As a result, a simple correlation provided in Table 2 can be utilized for these studies. Further parametric studies on the impact of parameters in the 3DOT simulation is left as future work.

3. Engineering-scale fission gas behavior model

Considering that U_3Si_2 under LWR conditions retains a polycrystalline structure, fission gas behavior is modeled as consisting of two main stages for intra-granular and inter-granular behavior, by analogy with UO_2 (e.g., Refs. [25,30,53–56]). The intra-granular component of the model (Section 3.1) includes the fundamental mechanisms of nucleation and re-resolution of intra-granular fission gas bubbles, gas atom trapping from the matrix into the bubbles, and gas atom diffusion to grain boundaries. The inter-granular component (Section 3.2) also adopts a mechanistic but relatively simple approach that encompasses grain-boundary bubble growth with inflow of gas atoms and vacancies, bubble coalescence, and fission gas release from the grain boundaries. The modeling approach is based on the concepts originally developed for UO_2 in Refs. [30,57]. However, the current model is tailored to the specific physical mechanisms and material properties for U_3Si_2 .

3.1. Intra-granular fission gas behavior model

The intra-granular component of the model provides the calculation of the gas diffusion rate to grain boundaries and of the intra-granular fission gas bubble swelling. The latter is computed based on a description of intra-granular bubble evolution in terms of number density and average size. A detailed description of intra-granular bubble evolution can be accomplished by employing cluster dynamics approaches to calculate the bubble size distribution and the evolution of the distribution over time. However, these detailed modeling approaches are computationally intensive and simpler models are normally used for engineering fuel performance code applications.

Following Clement and Wood [58], we derive our model starting from the detailed cluster dynamics representation, but we simplify the problem by considering only the moments of the size distribution of the clusters. Assuming that bubbles include all clusters containing two or more gas atoms, we define the total concentration of bubbles N (m^{-3}) and the mean of the size distribution \bar{n} ($/$), respectively

$$N = \sum_{n=2}^{\infty} c_n \quad (4)$$

$$\bar{n} = \frac{\sum_{n=2}^{\infty} n c_n}{N} \quad (5)$$

where c_n (at m^{-3}) is the number density of atom clusters (or bubbles) containing n atoms (with c_1 indicating the concentration of single gas atoms). The detailed cluster dynamics formulation of the master equations considered here is [59]

$$\begin{cases} \frac{\partial c_1}{\partial t} = D \nabla^2 c_1 + G - 2\nu + \alpha_2 c_2 - \sum_{n=2}^{\infty} \beta_n c_n + \sum_{n=3}^{\infty} \alpha_n c_n \\ \frac{\partial c_2}{\partial t} = D_2 \nabla^2 c_2 + \nu - (\beta_2 + \alpha_2) c_2 + \alpha_3 c_3 \\ \vdots \\ \frac{\partial c_n}{\partial t} = D_n \nabla^2 c_n + \beta_{n-1} c_{n-1} - (\beta_n + \alpha_n) c_n + \alpha_{n+1} c_{n+1} \end{cases} \quad (6)$$

where α_n (s^{-1}) represents the probability per second that an atom is re-solved from a cluster containing n atoms, β_n (s^{-1}) the probability per second that a single atom is trapped by a cluster containing n atoms, D_n ($\text{m}^2 \text{s}^{-1}$) is the diffusion coefficient of the cluster containing n atoms, ν ($\text{at m}^{-3} \text{s}^{-1}$) is the nucleation rate of fission gas dimers, and G ($\text{at m}^{-3} \text{s}^{-1}$) is the production rate of gas atoms. A schematic of the master equations governing the bubbles' nucleation, growth due to single atom trapping and shrinkage due to re-solution of single atoms in the fuel matrix is reported in Fig. 2.

The re-solution of gas atoms from the intra-granular bubbles into the fuel matrix is modeled as an irradiation-driven mechanism. Accordingly, we express the re-solution rate for U_3Si_2 as

$$\alpha = \alpha_0 \dot{F} \quad (7)$$

where α_0 (m^3) is a coefficient, which can in principle depend on the cluster size, and \dot{F} ($\text{m}^{-3} \text{s}^{-1}$) is the fission rate.

The trapping of gas atoms into intra-granular bubbles is modeled as a purely diffusion-driven process, and the trapping rate is calculated according to the formulation by Ham [60], considering immobile and dilute clusters

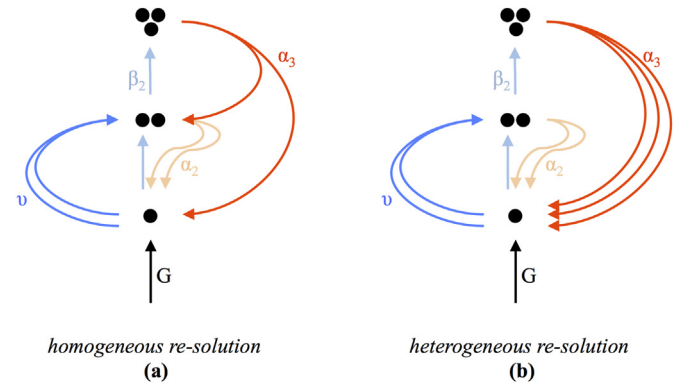


Fig. 2. Sketch of the mechanisms of cluster dynamics considering (a) homogeneous and (b) heterogeneous re-solution.

$$\beta_n = 4\pi D R_n c_1 \quad (8)$$

where D is the single gas atom diffusion coefficient in the fuel matrix, R_n (m) is the cluster size, and c_1 is the concentration of atoms in the matrix.

The nucleation of bubbles in U_3Si_2 is modeled as a diffusion-dependent process, consisting of dimer formation upon interaction of single gas atoms driven by atom diffusion in the matrix (so-called homogeneous nucleation [61,62]). The resulting nucleation rate can be expressed as [63].

$$\nu = 8\pi D R_{sg} f_n c_1^2 \quad (9)$$

where D is the diffusion coefficient of single gas atoms in the fuel matrix, R_{sg} (m) is the radius of a gas atom, and f_n ($/$) is the nucleation factor.

Combining Eqs. (5) and (6), we derive a single-size model consisting of expressions for the time evolution of N and \bar{n} , as follows. After algebraic summation, a first order Taylor expansion in the phase space is performed, namely

$$(\beta_n, \alpha_n, c_n) = (\beta(n), \alpha(n), c(n)) \approx (\beta_{\bar{n}}, \alpha_{\bar{n}}, c_{\bar{n}}) + \frac{\partial(\beta, \alpha, c)}{\partial n} dn \dots \quad (10)$$

Introducing the further assumption that the nucleation process occurs on a faster time scale compared to the growth process (i.e., $dN/dt \approx 0$ in the equation for $d\bar{n}/dt$), leads to

$$\begin{aligned} \frac{dN}{dt} &= \nu - \alpha_2 c_2 = \nu - \alpha_2 \phi N \\ \frac{d\bar{n}}{dt} &= \beta_{\bar{n}} - \alpha_{\bar{n}} \end{aligned} \quad (11)$$

where we account for the fact that homogeneous (i.e., by ejection of individual atoms) re-solution, in fact, results in complete bubble destruction if the re-solution event occurs for a dimer. The factor $\phi = c_2/N$ represents the fraction of dimers over the total number of bubbles. The term $\alpha_2 \phi$ represents the probability per second of bubble destruction applied to the total number density of clusters, N . A bubble of size \bar{n} will require on average $\bar{n} - 1$ homogeneous re-solution events before being destroyed. Considering this, in the single-size approach we estimate ϕ as

$$\phi = \frac{1}{\bar{n} - 1} \quad (12)$$

We define the total concentration of gas in bubbles, m (at m^{-3}), as

$$m = \bar{n}N \quad (13)$$

With the approximations of Eq. (10) and considering Eqs. (13) and (11), Eq. (6) reduce to

$$\begin{cases} \frac{dN}{dt} = \nu - \alpha\phi N \\ \frac{\partial c_1}{\partial t} = D\nabla^2 c_1 - \beta_{\bar{n}}N + \alpha\phi m + G - 2\nu \\ \frac{\partial m}{\partial t} = 2\nu + \beta_{\bar{n}}N - \alpha\phi m \end{cases} \quad (14)$$

Note that we introduced the additional assumption of immobile bubbles, with the diffusion term being considered for single gas atoms only. Differently from previous formulations of the single-size homogeneous model [62], the evolution of the bubble number density, N , considers also a term of bubble destruction, which corresponds to dimers affected by a homogeneous re-solution event. Moreover, homogeneous nucleation is consistently considered as a process of formation of dimers rather than considering nucleation at the average bubble size, which in previous work has been deemed as “the Achilles heel of the single-size method because it implies essentially instantaneous growth of dimers” to the average bubble size [62]. Hence, our model derived from a detailed cluster dynamics approach retains important bubble-distribution related effects in a formulation that in its final form only includes equations for the average quantities. Furthermore, the present model includes gas diffusion to grain boundaries in conjunction with bubble evolution.

The set of coupled partial differential equations (Eq. (14)) is solved using the recently developed PolyPole-2 algorithm [64], extended to the solution of the 3-equation system. Details of this extension are not given here for brevity, however, the concept of the algorithm is the same as described in Ref. [64].

3.1.1. Calculation of bubble size and swelling

The solution of Eq. (14) provides the bubble number density, the rate of single gas atom diffusion to grain boundaries, and the average number of atoms per bubble. While for UO_2 substantial experimental data is available, including data on the gas density in intra-granular bubbles that can be used to determine the average bubble size given the average number of gas atoms per bubble in a simple way [57,62], such information is missing for U_3Si_2 under LWR conditions. Therefore, we developed a physics-based approach to model intra-granular bubble growth considering the interactive gas atom and vacancy absorption at the bubbles, as follows.

Intra-granular fission gas bubbles are assumed spherical. The mechanical equilibrium of a spherical bubble is governed by the Young-Laplace equation

$$p_{eq} = \frac{2\gamma}{R_b} - \sigma_h \quad (15)$$

where p_{eq} (Pa) is the equilibrium pressure, γ (J m^{-2}) is the U_3Si_2 /gas specific surface energy and σ_h (Pa) is the hydrostatic stress (considered negative if the medium is under compression). In general, the bubbles are in a non-equilibrium state and tend to the equilibrium condition by absorbing or emitting vacancies. The bubble volume is calculated through

$$\frac{dV_b}{dt} = \omega \frac{dn^-}{dt} + \Omega \frac{dn_{iv}}{dt} \quad (16)$$

where V_b (m^3) is the bubble volume, ω (m^3) is the van der Waals atomic volume for xenon, and Ω (m^3) is the vacancy volume. The variation rate of the number of atoms per bubble, $d\bar{n}/dt$, is obtained from Eqs. (13) and (14). The vacancy absorption/emission rate at the bubble, dn_{iv}/dt , is calculated based on [65] as

$$\frac{dn_{iv}}{dt} = \frac{2\pi D_{ig}^v \rho}{kT\zeta} (p - p_{eq}) \quad (17)$$

where $n_{iv}()$ is the number of vacancies per intra-granular bubble, D_{ig}^v ($\text{m}^2 \text{s}^{-1}$) is the intra-granular vacancy diffusion coefficient, ρ (m) is the radius of the equivalent Wigner-Seitz cell² (e.g. Ref. [66]) surrounding a bubble, k (J K^{-1}) is the Boltzmann constant, T (K) is the local temperature, and $\zeta()$ is a dimensionless factor calculated as [67].

$$\zeta = \frac{10\psi(1 + \psi^3)}{-\psi^6 + 5\psi^2 - 9\psi + 5} \quad (18)$$

where $\psi = R_b/\rho$ is the ratio between the radii of the bubble and of the cell. The present model for vacancy absorption/emission at intra-granular bubbles is a reformulation of the Speight and Beere model for behavior at grain boundaries of bubbles of circular projection (2D problem) [56,65]. In particular, Eqs. (17) and (18) represent the equivalent model for vacancy absorption/emission at spherical bubbles in the bulk (3D problem). The different dimensionality of the problem yields a different expression for ζ relative to Refs. [56,65]. Eq. (18) was first derived in Ref. [67] for the problem of pore growth in the UO_2 high burnup structure.

Considering a rearranged formulation of the van der Waals equation of state³ and Eq. (16), the pressure of the gas in the bubble is

$$p = \frac{kT}{\Omega} \eta \quad (19)$$

where $\eta()$ is the ratio between \bar{n} and n_{iv} .

The intra-granular bubble radius is

$$R_b = \sqrt[3]{\frac{3V_b}{4\pi}} \quad (20)$$

Finally, the fractional volume change due to intra-granular fission gas swelling is calculated as

$$\left(\frac{\Delta V}{V}\right)_{ig} = V_b N \quad (21)$$

3.2. Inter-granular model

The inter-granular component of the model for fission gas behavior in U_3Si_2 is based on the model originally developed for UO_2 in Refs. [30,68], assuming that the same qualitative assumptions for gas behavior at grain boundaries apply to UO_2 and U_3Si_2 . In

² The radius of the Wigner-Seitz cell is determined from the relationship $4/3\pi N\rho^3 = 1$.

³ For xenon, the van der Waals equation of state can be reduced to Eq. (19), neglecting the pressure correction due to xenon covolume (e.g. Ref. [25]).

particular, we consider the development of a population of lenticular bubbles at grain faces, bubble coalescence during bubble growth, and fission gas release following saturation of the grain boundaries [30,56]. These similarities to UO_2 appear coherent when considering that both materials exhibit a polycrystalline structure under LWR conditions. They are also corroborated by the evidence from the metallographic images of U_3Si_2 irradiated at power reactor temperatures from Ref. [13].

The inter-granular model allows for the concurrent calculation of fission gas swelling due to grain-boundary bubbles and FGR through a direct description of bubble evolution [30]. The main features of the model are the following.

The absorption rate of gas at the grain-boundary bubbles is assumed to equal the arrival rate of gas at the grain boundaries [56,69]. An initial number density of grain-boundary bubbles, $N_{gf,0}$, is considered, and further nucleation during the irradiation is neglected (one-off nucleation, e.g. Ref. [56]). All grain-boundary bubbles are considered to have, at any instant, equal size and equal lenticular shape of circular projection. The flux of gas atoms from the grain boundaries to the grain interior by irradiation-induced re-solution of grain-boundary bubbles is neglected, in line with [30,70]. Grain-boundary bubble growth (or shrinkage) by inflow of gas atoms from within the grains and concomitant absorption (or emission) of vacancies from the grain boundaries is considered. The bubble growth/shrinkage rate is calculated as

$$\frac{dV_{gf}}{dt} = \omega \frac{dn_g}{dt} + \Omega \frac{dn_v}{dt} \quad (22)$$

where V_{gf} (m^3) is the bubble volume, ω (m^3) the van der Waals' volume of a fission gas atom, n_g (/) the number of fission gas atoms per bubble, Ω (m^3) the atomic (vacancy) volume in the bubble, and n_v (/) the number of vacancies per bubble. The gas atom inflow rate at the bubble, dn_g/dt , is obtained from Eq. (14). The vacancy absorption/emission rate at the bubble, dn_v/dt , is calculated using the model of Speight and Beere [65]

$$\frac{dn_v}{dt} = \frac{2\pi D_{gb}^v \delta_{gb}}{kTS} (p - p_{eq}) \quad (23)$$

where D_{gb}^v (m^2s^{-1}) is the vacancy diffusion coefficient along grain boundaries, δ_{gb} (m) the thickness of the diffusion layer in grain boundaries, and the parameter S ($-$)⁴ depends on the fraction of grain faces covered by bubbles (fractional coverage) as detailed in Ref. [56]. The pressure of the gas in the bubble, p (Pa), is calculated based on the van der Waals equation of state as [56]

$$p = \frac{kT}{\Omega} \frac{n_g}{n_v} \quad (25)$$

The mechanical equilibrium pressure, p_{eq} (Pa), is given by the sum of the bubble surface tension force and the hydrostatic stress in the surrounding medium (analogous to Eq. (15)). Given the volume (Eq. (22)) of a lenticular bubble of circular projection, the bubble radius of curvature is

⁴ As mentioned above, the parameter S depends on the geometrical representation of the emission/absorption phenomena. For behavior on a surface (grain boundary), the expression for S reads [56]

$$S = -\frac{(3 - F_c)(1 - F_c) + 2 \ln F_c}{4} \quad (24)$$

Where $F_c = N_{gf} A_{gf}$ ($-$) is the fractional coverage. Equation (24) is conceptually identical to Eq. (18), but considers an emission/absorption process constrained to a 2D geometry.

$$R_{gf} = \left(\frac{3V_{gf}}{4\pi\varphi(\theta)} \right)^{1/3} \quad (26)$$

where $\varphi = 1 - 1.5\cos(\theta) + 0.5\cos^3(\theta)$ is the geometric factor relating the volume of a lenticular bubble to that of a sphere, and θ is the bubble semi-dihedral angle.

Grain-boundary bubble coalescence is described using an improved model of White [30,56]. The variation rate of the bubble number density, N_{gf} (m^{-2}), due to coalescence is calculated as a function of the variation rate of the bubble projected area on the grain face, $A_{gf} = \pi R_{gf}^2$ (m^2). More details are given in Ref. [30]. A lower limit, $N_{gf,low} = 10^{10} \text{m}^{-2}$ is set.

Under the above assumptions, the fractional fuel volume change due to grain-boundary fission gas swelling is calculated at each time step as

$$\frac{\Delta V}{V} = \frac{1}{2} \frac{3}{r_{gr}} N_{gf} V_{gf} \quad (27)$$

where V (m^3) is the fuel volume, r_{gr} (m) the grain radius, and $3/r_{gr}$ represents the grain surface to volume ratio.

Thermal FGR is modeled based on a principle of grain face saturation. More precisely, after the fractional coverage attains a saturation value, $F_{c,sat}$, further bubble growth is compensated by gas release in order to maintain the constant coverage condition

$$\frac{dF_c}{dt} = -\frac{d(N_{gf} A_{gf})}{dt} = 0 \quad \text{if } F_c = F_{c,sat} \quad (28)$$

Note that fission gas release and swelling are described as inherently coupled phenomena, as fission gas release from the grain faces counteracts bubble growth and thereby fission gas swelling. In the absence of specific experimental data for the saturation coverage in U_3Si_2 , we choose $F_{c,sat} = \pi/4$, which corresponds to the theoretical, geometrical interlinkage condition for uniformly arranged bubbles of circular projection. This value has been used also for UO_2 [71], although more recent models generally adopt a lower value of 50% that is based on the empirical evidence available for UO_2 [56]. A specific investigation of the saturation coverage in U_3Si_2 , e.g., by means of meso-scale techniques such as phase field modeling, would be useful to provide a more accurate saturation threshold. This improvement is being pursued in the near future. Also, at this stage, the model does not take into account the effect of as-fabricated porosity in fission gas behavior, i.e., gas trapping at fabrication pores.

3.3. Values for the model parameters

Nominal values and correlations used for the parameters of the model presented in Sections 3.1 and 3.2 are summarized in Table 2. These values are based either on the lower-length scale calculations performed in the present work (Section 2) or on information available from the literature. As significant uncertainties still exist in many of the parameters, a sensitivity analysis is performed in Section 5.

The adopted single gas atom diffusion coefficient, D is the one for the migration of Xe in a U (U 2a) vacancy assisted by a second U 2a vacancy along the c axis of the ideal U_3Si_2 unit cell. Indeed, this is the dominant mechanism over the temperatures of interest for LWR applications, as it is associated with a larger diffusivity compared to the other processes, as discussed in Section 2.1. For analogous reasons, for the intra-granular vacancy diffusion coefficient, D_{ig}^v , we chose the one for the U (U 2a) vacancy diffusion along the c-axis.

The nucleation factor, f_n , represents a sort of nucleation efficiency, i.e., the probability that, after impinging, two atoms actually form a dimer. For this parameter, we adopt a value within the accepted range for UO_2 , e.g., Ref. [72]. Indeed, the nucleation factor is one of the most uncertain parameters (even for UO_2), and specific information for U_3Si_2 is missing. Investigation of the impact of this parameter on the results is included in the sensitivity analysis presented in Section 5.

To the best of our knowledge, no values for the grain-boundary vacancy diffusion coefficient, D_{gb}^v , for U_3Si_2 under LWR conditions are available at this time. As a preliminary approach, we choose to employ the intra-granular vacancy diffusion coefficient derived in Section 2.1 and reported in Table 2, multiplied by a scaling factor equal to 10^6 . The magnitude of the scaling factor is related to atomic jump frequencies at grain boundaries, which are roughly 10^6 times higher than jump frequencies for lattice atoms [69].

For the semi-dihedral angle of grain-boundary bubbles, we tentatively use a value of 50° , commonly accepted for UO_2 (e.g. Ref. [56]). Using a specific U_3Si_2 value, which can be derived from recent molecular dynamics calculations of grain boundary and surface energies in Ref. [74], is planned for the near future.

4. Irradiation experiment simulation

In this Section, we present and discuss the simulation of the U_3Si_2 irradiation experiment from Shimizu [13]. To the best of the authors' knowledge, this is the only in-pile experiment on U_3Si_2 fuel under temperatures and irradiation conditions compatible with commercial LWRs and whose details and data are available in the open literature. The simulation is intended to demonstrate a physically meaningful representation of fission gas behavior of U_3Si_2 under LWR conditions with the model presented in Section 3. The more substantial validation of the model will require a larger amount of experimental data and will be the subject of future work as new experiments are performed, e.g., in the framework of the AFC.

4.1. Description of the analyzed experiment

The considered experiment, referred to as AI-7-1 [13], was performed by Atomics International to determine U_3Si_2 irradiation behavior characteristics, i.e., dimensional stability and fission gas release. The irradiation involved a single fuel rod. The fuel column (H30.5 cm, \varnothing 0.889 cm) was made of six slugs of 10% ^{235}U enriched, slightly hypo-stoichiometric U_3Si_2 . The cladding was stainless steel (SS 304) and the gap between the fuel and the cladding was filled with sodium to provide efficient heat transfer. The fuel was irradiated to a maximum average burnup of 7.3 GWd tU^{-1} at a power of 46 kW m^{-1} with maximum center and surface temperatures of 1230 K and 970 K, respectively.

In particular, in this work we focus on one of the slugs composing the fuel column, labelled as specimen #14, whose irradiation conditions are summarized in Table 3. We chose to focus on this slug for several reasons:

Table 3

Irradiation conditions for the fuel slug labelled specimen #14 from the AI-7-1 irradiation experiment.

Irradiation conditions	
Fresh fuel stoichiometry (wt.%)	7.08
Linear heat rate (kW m^{-1})	37.4
Burnup (GWd tU^{-1})	6.0
Average centerline temperature (K)	1050
Average surface temperature (K)	850

Table 4

Post-irradiation examination and image analysis results for fuel slug #14 from the AI-7-1 irradiation experiment.

Quantity	Value	Reference
Final local fuel stoichiometry (wt.%)	6.79	[13]
Overall density variation (%)	−12.6	[13]
Specimen length variation (%)	3.0	[13]
Specimen diameter variation (%)	3.0	[13]
Fission gas release (%)	2.6	[13]
Final grain radius, 3D (μm)	28 ± 7	[75]
Intra-granular gaseous swelling (%)	2.9	[75]
Inter-granular gaseous swelling (%)	9.2	[75]

- The specimen did not crack under irradiation, allowing for higher precision in determining the dimensional changes of the fuel.
- The thermocouple installed near the slug exhibited a stable behavior throughout the irradiation, enabling a proper estimation of local fuel temperature.
- After irradiation, the slug was sectioned and a metallographic image in the fuel central region was taken. Based on this metallographic image, an estimation of local fuel swelling due to fission gas bubbles was possible and has been performed [75].

Detailed post-irradiation examinations (PIE), have been produced during the experimental campaign. Those data have been complemented by recent image analyses to determine gaseous swelling and grain size [75]. The original PIE data reported by Shimizu on specimen #14, together with the recent data from image analysis according to Ref. [75], are reported in Table 4. This first set of experimental data is used here for comparison with model calculations.

4.2. Setup of calculations

We performed the calculations using a stand-alone C++ code for the fission gas behavior model presented in Section 3. The irradiation conditions applied in our simulation are coherent with those reported in Ref. [13] and summarized in Table 3. In particular, we performed a local analysis for the centerline portion of the specimen, where local experimental data from image analysis [75] are available. Local temperature considered for the simulation is 1050 K (Table 3).

4.3. Results and discussion

In Fig. 3, we compare the results of our simulations in terms of fission gas release and gaseous swelling to the experimental data. FGR is defined as the ratio of the released to generated gas, whereas gaseous swelling is calculated as defined in Section 3 and is the sum of the intra- and inter-granular contributions. FGR (dashed-blue line) exhibits an incubation behavior [76], with no release being observed until the grain-boundary bubble coverage attains a saturation level. Also, as fission gas swelling and release are described as inherently coupled in the model (Section 3.2), a change of the swelling rate can be observed at the onset of FGR. In particular, the swelling rate is reduced by the loss of gas from the grain faces as FGR takes place. The agreement between calculations and the experimental results appears reasonable for a preliminary model. Note that the FGR comparison is not fully consistent, as the calculation refers to the centerline (hottest) portion of the specimen only. As expected, FGR is thus over-estimated.

In Fig. 4, we show results specific to the intra-granular model (Section 3.1). In particular, the calculated number density and radius

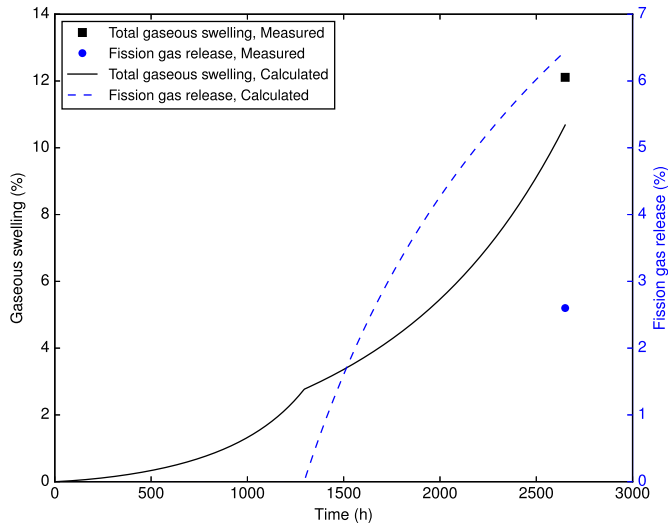


Fig. 3. FGR and total gaseous swelling as a function of irradiation time for specimen # 14 of the Al-7-1 experiment. Calculation results and experimental data are included.

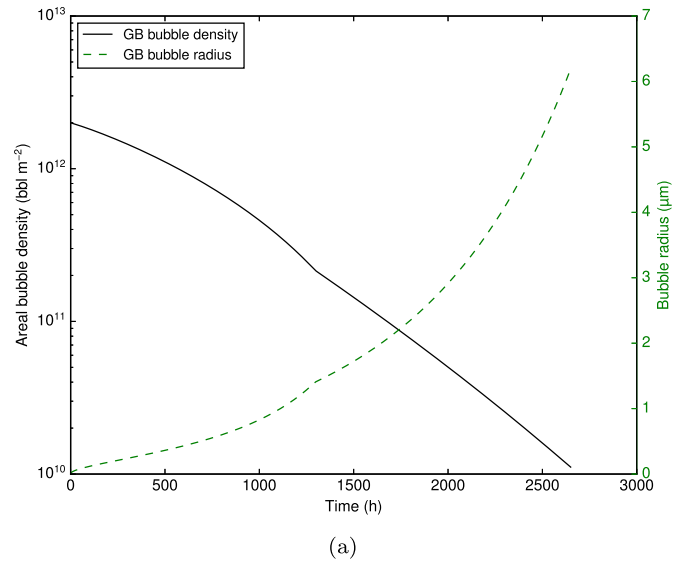


Fig. 4. Calculated volumetric number density and radius of intra-granular (IG) bubbles as a function of irradiation time for specimen # 14 of the Al-7-1 experiment.

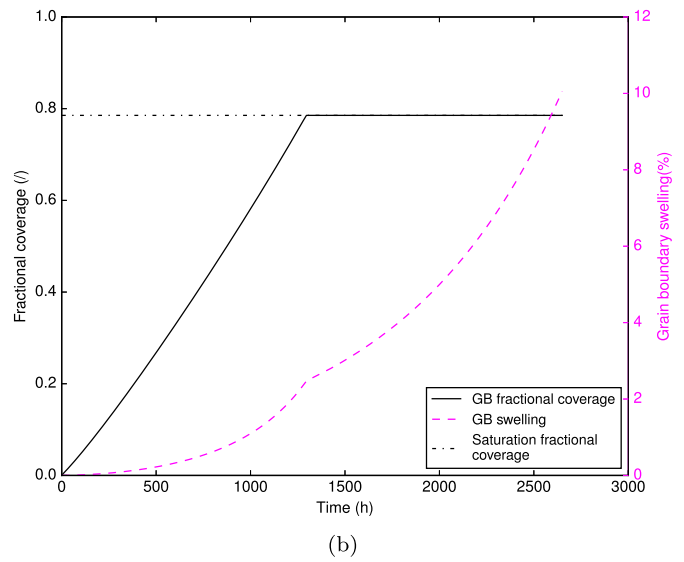


Fig. 5. Calculated areal number density and radius of curvature (a) of grain-boundary (GB) bubbles as a function of time for specimen # 14 of the Al-7-1 experiment. Grain-boundary fractional coverage and swelling (b) as a function of time. The saturation fractional coverage of $\pi/4$ [71] is also reported.

Table 5

Parameters considered in the sensitivity analysis and corresponding ranges of variation.

Parameter	Nominal value	Scaling factor range
Intra-granular diffusion coefficient, atoms (m s^{-2})	$5.91 \cdot 10^{-6} \exp(-4.41 \cdot 10^{-19}/kT)$	[0.1; 10]
Intra-granular diffusion coefficient, vacancies (m s^{-2})	$3.35 \cdot 10^{-6} \exp(-4.63 \cdot 10^{-19}/kT)$	[0.1; 10]
Nucleation factor (I)	10^{-4}	$[10^{-5}; 10^2]$
Re-solution rate (s^{-1})	$2.80 \cdot 10^{-25} \left(\frac{5 \cdot 10^{-10}}{R_b} \right)^{0.23} \cdot \dot{F}$	[0.1; 10]
$\text{U}_3\text{Si}_2/\text{gas}$ specific surface energy (J m^{-2})	1.16	[0.5; 1.5]
Inter-granular diffusion coefficient, vacancies (m s^{-2})	$10^6 \cdot D_{\text{ig}}^v$	$[10^{-2}; 10^2]$
Inter-granular bubbles initial number (bbl m^{-2})	$2 \cdot 10^{12}$	$[10^{-3}; 10^3]$
Inter-granular bubbles dihedral angle (deg)	50	[0.5; 1.5]
Saturation coverage of grain faces (I)	$\pi/4$	$\left[\frac{2}{\pi}; 1 \right]$

of intra-granular fission gas bubbles are shown. The results point out a lower number density and a higher radius of intra-granular bubbles compared to UO_2 under operational LWR conditions (e.g. Refs. [57,62]). This appears consistent with the metallographic images from Ref. [13] and with the higher diffusivities of gas atoms and vacancies in U_3Si_2 compared to UO_2 as indicated by the lower-length scale calculations performed in this work (Section 2).

Fig. 5 illustrates results specific to the inter-granular model (Section 3.2). In Fig. 5a, we show the time evolution of the areal number density and radius of curvature of grain-boundary fission gas bubbles. The decrease in the bubble density is due to the progressive bubble coalescence during growth. Correspondingly, the bubble radius increases. The evolution during irradiation of grain-boundary fractional coverage and grain-boundary swelling are illustrated in Fig. 5b. FGR commences at the attainment of saturation coverage (see Fig. 3), and the swelling rate correspondingly decreases.

5. Sensitivity analysis

The irradiation experiment simulation presented in Section 4 is complemented with a sensitivity analysis aimed at assessing the impact on the results of the model parameters. This sensitivity analysis is essential for at least two reasons: (i) in view of the lack of data for U_3Si_2 , in the selection of some parameters (i.e., nucleation factor, diffusion coefficient of vacancies at grain boundaries, inter-granular bubbles dihedral angle) assumptions were made; (ii) a sensitivity analysis can provide guidance for future research on characterization of the physical mechanisms and the associated engineering parameters, including both experimental and lower-length scale modeling efforts. In this Section, we present the methodology employed for the sensitivity analysis and discuss the results obtained.

The parameters considered in the sensitivity analysis are reported in Table 5 along with the considered nominal values and ranges of variation. We performed the analysis for various temperatures, i.e., from 800 to 1200 K at intervals of 50 K. For the other boundary conditions (including irradiation time, fission rate, grain size) we adopted the same as in Section 4. For each one of the considered temperatures, we performed 10,000 simulations, randomly sampling the scaling factors in the ranges specified in Table 5, i.e., adopting a Monte Carlo approach. Uniform distributions were assumed for the parameters. The tool employed to carry out the sensitivity analysis is the RAVEN statistical analysis framework [77,78], developed at INL. Considered figures of merit for the analysis are calculated fission gas release, intra-granular swelling, and inter-granular swelling.

In Figs. 6–8, we show the results of the sensitivity analysis in terms of Pearson correlation coefficient and normalized sensitivity coefficient on the three selected outputs, namely fission gas release, intra- and inter-granular swelling. The Pearson coefficient indicates how strong the correlation of a certain parameter is with respect to the chosen figure of merit, while the normalized sensitivity coefficient provides a measure of the relative variation of the figure of merit with respect to the variation of a specific parameter.

The re-resolution rate and the intra-granular nucleation factor exhibit a strong correlation with FGR (Fig. 6) on the whole temperature range considered, as they are characterized by the highest Pearson coefficient. However, only the re-resolution rate is associated with an appreciable sensitivity coefficient. Results suggest that the choice of the nucleation factor, which involved a strong assumption based on the experience on UO_2 , has nevertheless a low impact on the calculation results.

As shown in Fig. 7, the calculated intra-granular swelling results

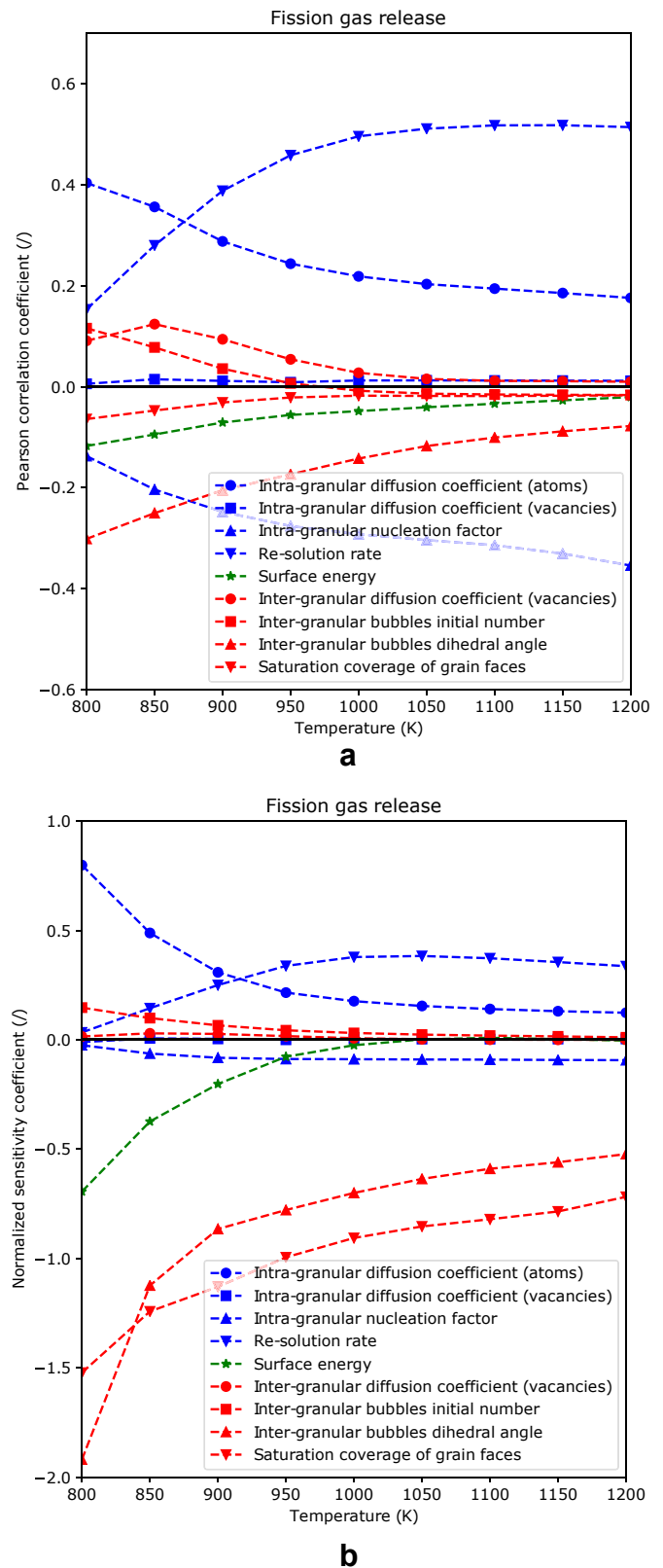


Fig. 6. Pearson coefficient (a) and normalized sensitivity coefficient (b) of the selected parameters to fission gas release at various temperatures.

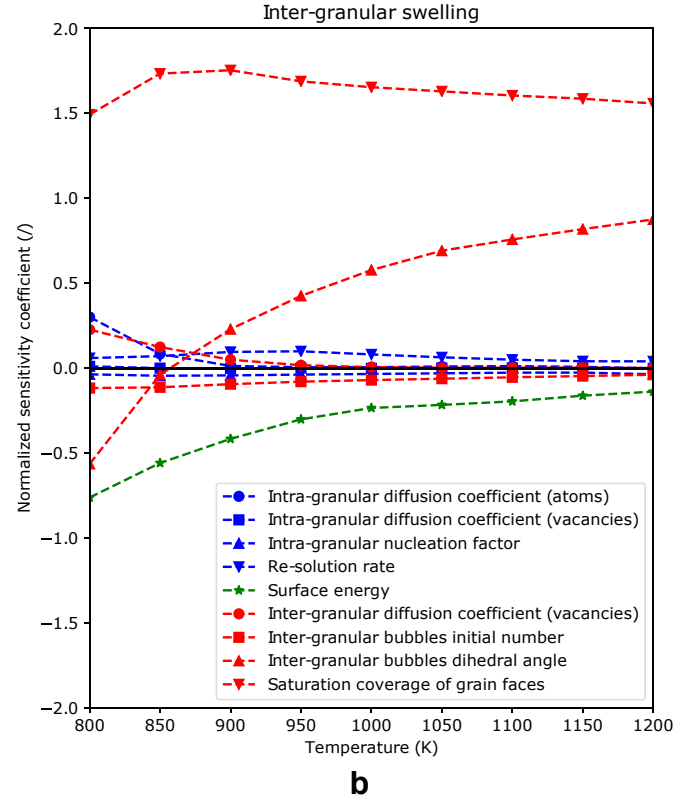
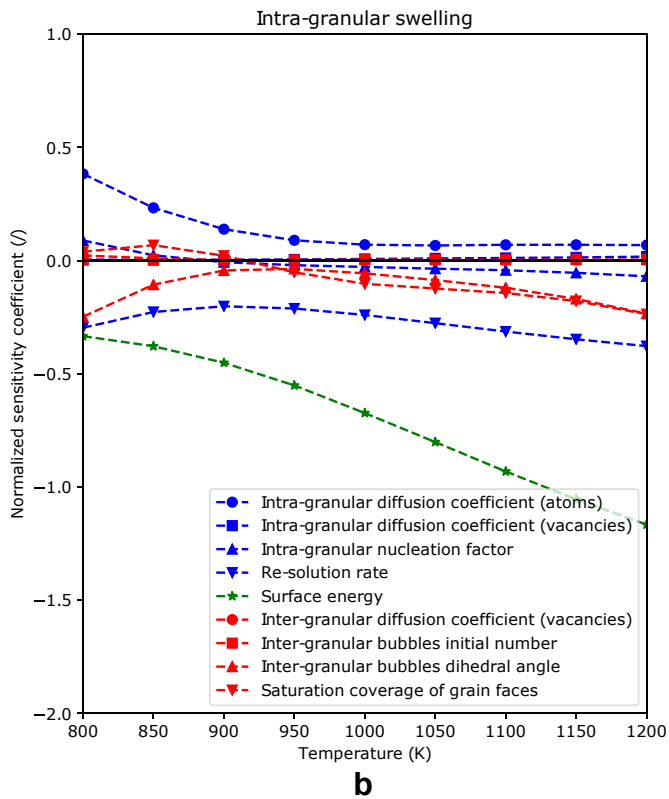
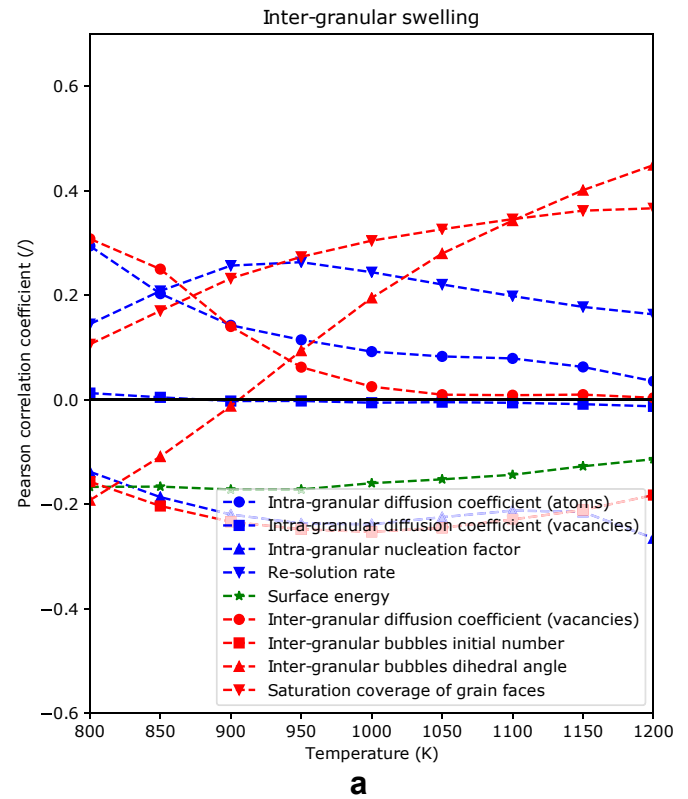
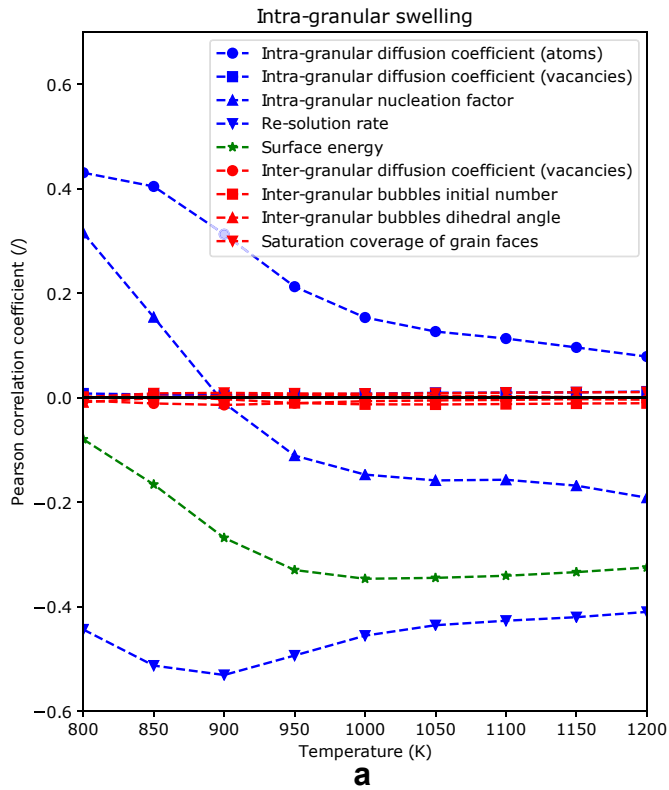


Fig. 7. Pearson coefficient (a) and normalized sensitivity coefficient (b) of the selected parameters to intra-granular gaseous swelling at various temperatures.

Fig. 8. Pearson coefficient (a) and normalized sensitivity coefficient (b) of the selected parameters to inter-granular gaseous swelling at various temperatures.

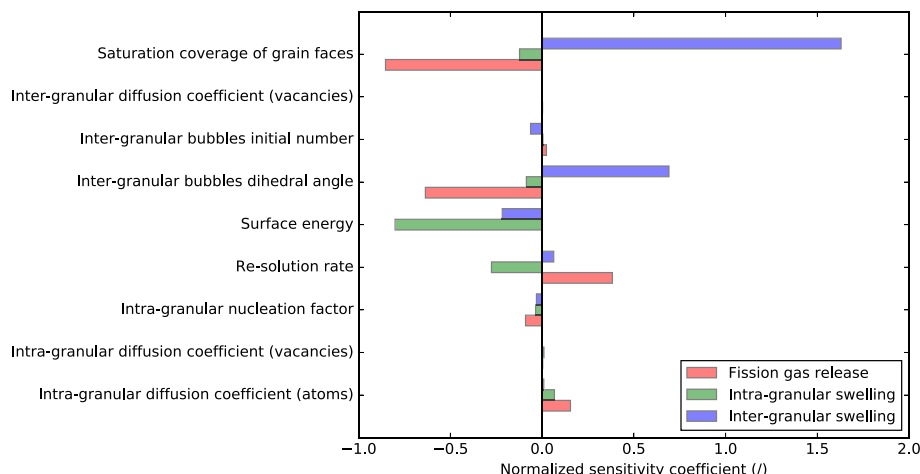


Fig. 9. Normalized sensitivity coefficients of the selected parameters to fission gas release, intra- and inter-granular swelling at the temperature of 1050 K.

are mostly sensitive to the re-resolution rate and specific surface energy, while the dominant parameters for the calculated inter-granular swelling (Fig. 8) are the grain-boundary bubbles dihedral angle and saturation coverage. The estimation of the saturation coverage in U_3Si_2 through phase field techniques or experimental measurements, complemented by the recent molecular dynamics calculations for grain boundary and surface energies [74], will be used to improve the presented inter-granular model in the near future.

In Fig. 9, we show the sensitivity coefficients calculated at the same temperature as the simulation in Section 4, i.e., 1050 K. It is noted that the vacancy diffusion coefficients are associated with low sensitivity coefficients, indicating that both intra- and inter-granular bubbles rapidly reach the equilibrium pressure and size (Section 3) due to the high mobility of vacancies in U_3Si_2 according to the adopted diffusivity model.

6. Conclusions

In this work, we presented a model for fission gas behavior in U_3Si_2 under LWR conditions. The model includes components for intra-granular and grain-boundary behavior of fission gases and describes the evolution of fission gas bubbles within the grains and at grain boundaries, intra-granular gas atom diffusion, and fission gas release. In order to fill the gap in the experimental data available for U_3Si_2 under LWR conditions, we adopted a multiscale approach whereby lower-length scale modeling for the parameters is used to inform the engineering scale calculation. In particular, we derived the intra-granular single gas atom diffusion coefficient and point defect properties through DFT calculations, and the re-resolution parameter through BCA calculations. The model was applied to the simulation of an experiment for U_3Si_2 at power reactor temperatures available in the literature, pointing out a physically meaningful representation of fission gas swelling and release. Moreover, we carried out a sensitivity analysis to assess the importance of various model parameters in the calculated fission gas swelling and release. On the one hand, the saturation coverage of grain faces, the re-resolution parameter, and the U_3Si_2 /gas specific surface energy emerged as a set of high-priority parameters to be further investigated. On the other, the sensitivity analysis indicated that some of the most uncertain parameters of the model, i.e. the intra-granular nucleation factor and the grain-boundary vacancy diffusion coefficient, are associated with weak Pearson and sensitivity coefficients over the considered temperature range.

We conclude that the work (i) demonstrated an operational multiscale modeling approach for fission gas behavior in U_3Si_2 , (ii) provided a modeling framework with a promising potential for the calculation of fission gas swelling and release in U_3Si_2 under LWR conditions for engineering fuel analysis, and (iii) provided indications that can help addressing future research on the characterization of the parameters through a sensitivity analysis. The model can be progressively improved as new data become available from theoretical and experimental research. The model of fission gas behavior in U_3Si_2 under LWR conditions presented in this paper is currently available in the BISON fuel performance code of Idaho National Laboratory.

Further developments of the model will involve the incorporation of improved parameters from new atomistic and meso-scale calculations. These will include, in particular, updated models for the diffusivities of fission gas atoms and vacancies in the U_3Si_2 lattice, also accounting for irradiation-driven diffusion of fission gas atoms, as well as improved estimates for the grain-boundary bubble coverage at saturation and for grain-boundary and surface energies.

Acknowledgments

This work was funded by the US Department of Energy through the Nuclear Energy Advanced Modeling and Simulation (NEAMS) program and the Consortium for Advanced Simulation of Light Water Reactors (CASL). The submitted manuscript has been authored by a contractor of the U.S. Government under Contract DE-AC07-05ID14517. Accordingly, the U.S. Government retains a non-exclusive, royalty free license to publish or reproduce the published form of this contribution, or allow others to do so, for U.S. Government purposes.

Appendix A. Supplementary data

Supplementary data to this article can be found online at <https://doi.org/10.1016/j.jnucmat.2019.04.037>.

References

- [1] S. Zinkle, K. Terrani, J. Gehin, L. Ott, L. Snead, Accident tolerant fuels for LWRs: a perspective, *J. Nucl. Mater.* 448 (1) (2014) 374–379.
- [2] S. Bragg-Sitton, B. Merrill, M. Teague, L. Ott, K. Rob, M. Farmer, M. Billone, R. Montgomery, C. Stanek, M. Todosow, N. Brown, Advanced Fuels Campaign Light Water Reactor Accident Tolerant Fuel Performance Metrics, 2014. Tech. Rep., INL/EXT-13-29957.

- [3] H.-G. Kim, J.-H. Yang, W.-J. Kim, Y.-H. Koo, Development status of accident-tolerant fuel for light water reactors in Korea, *Nucl. Eng. Technol.* 48 (1) (2016) 1–15.
- [4] State-of-the-Art Report on Light Water Reactor Accident-Tolerant Fuels, November 2018, p. 372. <https://doi.org/https://doi.org/10.1787/9789264308343-en>. Tech. Rep., OECD/NEA No. 7317.
- [5] J. White, A. Nelson, D. Byler, J. Valdez, K. McClellan, Thermophysical properties of U_3Si to 1150 K, *J. Nucl. Mater.* 452 (1) (2014) 304–310.
- [6] J. White, A. Nelson, J. Dunwoody, D. Byler, D. Safarik, K. McClellan, Thermophysical properties of U_3Si_2 to 1773 K, *J. Nucl. Mater.* 464 (2015) 275–280.
- [7] J. Wood, M. Foo, L. Berthiaume, L. Herbert, J. Schaefer, Advances in the manufacturing and irradiation of reduced enrichment fuels for Canadian research reactors, in: Proc. of the Int. Meeting on Reduced Enrichment Fuels for Research and Test Reactors, Tokai, Japan, October, no. JAERI-M-84-073, 1983.
- [8] J. Snelgrove, R. Domagala, G. Hofman, T. Weincek, G. Copeland, R. Hobbs, R. Senn, The Use of U_3Si_2 Dispersions in Aluminum in Plate-Type Fuel Elements for Research and Test Reactors, 1987. Tech. Rep. ANL/RERTR/TM-11.
- [9] W. Krug, E. Groos, J. Seferiadis, Thamm, final results of test-irradiations with LEU-plats at KFA jülich, in: Proc. of the Int. Meeting on Reduced Enrichment Fuels for Research and Test Reactors, San Diego, California, USA, 19–22 September, 1988.
- [10] M. Ugajin, M. Akabori, A. Itoh, H. Someya, T. Nakagawa, K. Ohsawa, Capsule irradiation tests of U-Si and U-me (Fe,Ni,Mn) alloys for use in research reactors, in: Proc. of the Int. Meeting on Reduced Enrichment Fuels for Research and Test Reactors, Oarai, Ibaraki, Japan, October, 1993.
- [11] D. Sears, M. Primeau, C. Buchanan, D. Rose, Post-irradiation examination of prototype Al-64 wt% U_3Si_2 fuel rods from NRU, in: Proc. of the Int. Meeting on Reduced Enrichment Fuels for Research and Test Reactors, Williamsburg, Virginia, USA, vols. 18–23, 1994. September.
- [12] A. Leenaers, S. Van Den Bergh, E. Koonen, P. Jacquet, C. Jalousie, B. Guigon, A. Ballagny, L. Sannen, Microstructure of U_3Si_2 fuel plates submitted to a high heat flux, *J. Nucl. Mater.* 327 (2–3) (2004) 121–129.
- [13] H. Shimizu, The Properties and Irradiation Behavior of U_3Si_2 , Tech. Rep. NAA-SR-10621, Atomics International, 1965, <https://doi.org/10.2172/4639974>.
- [14] J.M. Harp, F. Cappia, Accident tolerant fuels (ATF-1) irradiation tests: overview of the ongoing post-irradiation examinations, in: 2018 ANS Annual Meeting, Philadelphia, USA, 2018.
- [15] G. Hofman, Crystal structure stability and fission gas swelling in intermetallic uranium compounds, *J. Nucl. Mater.* 140 (3) (1986) 256–263.
- [16] R. Birtcher, J. Richardson Jr., M. Mueller, Amorphization of U_3Si by ion or neutron irradiation, *J. Nucl. Mater.* 244 (3) (1997) 251–257.
- [17] M.R. Finlay, G.L. Hofman, J.L. Snelgrove, Irradiation behaviour of uranium silicide compounds, *J. Nucl. Mater.* 325 (2–3) (2004) 118–128.
- [18] R.C. Birtcher, J.W. Richardson, M.H. Mueller, Amorphization of U_3Si_2 by ion or neutron irradiation, *J. Nucl. Mater.* 230 (2) (1996) 158–163.
- [19] Y.S. Kim, G.L. Hofman, J. Rest, A.B. Robinson, Temperature and dose dependence of fission-gas-bubble swelling in U_3Si_2 , *J. Nucl. Mater.* 389 (3) (2009) 443–449.
- [20] Y. Miao, J. Harp, K. Mo, S. Bhattacharya, P. Baldo, A.M. Yacout, Short Communication on "In-situ TEM ion irradiation investigations on U_3Si_2 at LWR temperatures", *J. Nucl. Mater.* 484 (2017) 168–173.
- [21] Y. Miao, J. Harp, K. Mo, S. Zhu, T. Yao, J. Lian, A.M. Yacout, Bubble morphology in U_3Si_2 implanted by high-energy Xe ions at 300°C, *J. Nucl. Mater.* 495 (2017) 146–153.
- [22] Y. Miao, J. Harp, K. Mo, S. Zhu, T. Yao, A.M. Yacout, Bubble morphology in U_3Si_2 implanted by high-energy Xe ions at 600°C, *J. Nucl. Mater.* (2017) 1–9.
- [23] T. Yao, B. Gong, L. He, J. Harp, M. Tonks, J. Lian, Radiation-induced grain subdivision and bubble formation in U_3Si_2 at LWR temperature, *J. Nucl. Mater.* 498 (2018) 169–175.
- [24] T. Yao, B. Gong, L. He, Y. Miao, J.M. Harp, M. Tonks, J. Lian, In-situ TEM study of the ion irradiation behavior of U_3Si_2 and U_3Si , *J. Nucl. Mater.* 511 (2018) 56–63.
- [25] D.R. Olander, Fundamental Aspects of Nuclear Reactor Fuel Elements, Technical Information Center – Energy Research and Development Administration, University of California, Berkeley, CA, USA, 1976.
- [26] J. Rest, A model for fission-gas-bubble behavior in amorphous uranium silicide compounds, *J. Nucl. Mater.* 325 (2004) 107–117.
- [27] Y. Miao, K.A. Gamble, D. Andersson, B. Ye, Z.G. Mei, G. Hofman, A.M. Yacout, Gaseous swelling of U_3Si_2 during steady-state LWR operation: a rate theory investigation, *Nucl. Eng. Des.* 322 (2017) 336–344.
- [28] J. Rest, GRASS-SST: a Comprehensive Mechanistic Model for the Prediction of Fission-Gas Behavior in UO_2 -Base Fuels during Steady-State and Transient Conditions, Tech. Rep. ANL-78-53, 1978.
- [29] R.L. Williamson, J.D. Hales, S.R. Novascone, M.R. Tonks, D.R. Gaston, C.J. Permann, D. Andrs, R.C. Martineau, Multidimensional multiphysics simulation of nuclear fuel behavior, *J. Nucl. Mater.* 423 (2012) 149–163.
- [30] G. Pastore, L. Luzzi, V. Di Marcello, P. Van Uffelen, Physics-based modelling of fission gas swelling and release in UO_2 applied to integral fuel rod analysis, *Nucl. Eng. Des.* 256 (2013) 75–86.
- [31] M. Stan, Discovery and design of nuclear fuels, *Mater. Today* 12 (11) (2009) 20–28.
- [32] E. Kotomin, Y. Mastrikov, S. Rashkeev, P. Van Uffelen, Implementing first principles calculations of defect migration in a fuel performance code for UN simulations, *J. Nucl. Mater.* 393 (2) (2009) 292–299.
- [33] D. Andersson, P. Garcia, X.-Y. Liu, G. Pastore, M. Tonks, P. Millett, B. Dorado, D. Gaston, D. Andrs, R. Williamson, R. Martineau, B. Uberuaga, C. Stanek, Atomistic modeling of intrinsic and radiation-enhanced fission gas (Xe) diffusion in UO_{2+x} : implications for nuclear fuel performance modeling, *J. Nucl. Mater.* 451 (1) (2014) 225–242.
- [34] M.R. Tonks, X.Y. Liu, D. Andersson, D. Perez, A. Chernatynskiy, G. Pastore, C.R. Stanek, R. Williamson, Development of a multiscale thermal conductivity model for fission gas in UO_2 , *J. Nucl. Mater.* 469 (2016) 89–98.
- [35] D. Andersson, X.-Y. Liu, B. Beeler, S. Middleburgh, A. Caisse, C. Stanek, Density functional theory calculations of self- and Xe diffusion in U_3Si_2 , *J. Nucl. Mater.* 515 (2019) 312–325.
- [36] G. Kresse, J. Furthmüller, Efficiency of ab-initio total energy calculations for metals and semiconductors using a plane-wave basis set, *Comput. Mater. Sci.* 6 (1) (1996) 15–50.
- [37] G. Kresse, D. Joubert, From ultrasoft pseudopotentials to the projector augmented-wave method, *Phys. Rev. B* 59 (1999) 1758–1775.
- [38] S.L. Dudarev, D. Nguyen Manh, A.P. Sutton, Effect of Mott-Hubbard correlations on the electronic structure and structural stability of uranium dioxide, *Phil. Mag. B* 75 (5) (1997) 613–628.
- [39] M.J. Noordhoek, T.M. Besmann, D.A. Andersson, S.C. Middleburgh, A. Chernatynskiy, Phase equilibria in the U-Si system from first-principles calculations, *J. Nucl. Mater.* 479 (2016) 216–223.
- [40] S. Middleburgh, R. Grimes, E. Lahoda, C. Stanek, D. Andersson, Non-stoichiometry in U_3Si_2 , *J. Nucl. Mater.* 482 (2016) 300–305.
- [41] G. Mills, H. Jönsson, G.K. Schenter, Reversible work transition state theory: application to dissociative adsorption of hydrogen, *Surf. Sci.* 324 (2) (1995) 305–337.
- [42] D.A. Andersson, B.P. Uberuaga, P.V. Nerikar, C. Unal, C.R. Stanek, U and Xe transport in UO_{2+x} : density functional theory calculations, *Phys. Rev. B* 84 (2011), 054105.
- [43] R.S. Nelson, The stability of gas bubbles in an irradiation environment, *J. Nucl. Mater.* 31 (2) (1969) 153–161.
- [44] J.A. Turnbull, The distribution of intragranular fission gas bubbles in UO_2 during irradiation, *J. Nucl. Mater.* 38 (2) (1971) 203–212.
- [45] H. Blank, Properties of fission spikes in UO_2 and UC due to electronic stopping power, *Phys. Status Solidi* 10 (2) (1972) 465–478.
- [46] H. Blank, H. Matzke, The effect of fission spikes on fission gas re-solution, *Radiat. Eff.* 17 (1–2) (1973) 57–64.
- [47] C. Ronchi, P.T. Elton, Radiation re-solution of fission gas in uranium dioxide and carbide, *J. Nucl. Mater.* 140 (3) (1986) 228–244.
- [48] C. Matthews, D. Schwen, A.C. Klein, Radiation re-solution of fission gas in non-oxide nuclear fuel, *J. Nucl. Mater.* 457 (C) (2015) 273–278.
- [49] D.C. Parfitt, R.W. Grimes, Predicted mechanisms for radiation enhanced helium resolution in uranium dioxide, *J. Nucl. Mater.* 381 (3) (2008) 216–222.
- [50] D. Schwen, M. Huang, P. Bellon, R.S. Averback, Molecular dynamics simulation of intragranular Xe bubble re-solution in UO_2 , *J. Nucl. Mater.* 392 (1) (2009) 35–39.
- [51] K. Govers, C.L. Bishop, D.C. Parfitt, S.E. Lemehov, M. Verwerft, R.W. Grimes, Molecular dynamics study of Xe bubble re-solution in UO_2 , *J. Nucl. Mater.* 420 (1–3) (2012) 282–290.
- [52] J.F. Ziegler, J.P. Biersack, The stopping and range of ions in matter, in: Treatise on Heavy-Ion Science, Springer US, Boston, MA, 1985, pp. 93–129.
- [53] R.J. White, M.O. Tucker, A new fission-gas release model, *J. Nucl. Mater.* 118 (1) (1983) 1–38.
- [54] K. Forsberg, A.R. Massih, Fission gas release under time-varying conditions, *J. Nucl. Mater.* 127 (1985) 141–145.
- [55] A.R. Massih, K. Forsberg, Calculation of grain boundary gaseous swelling in UO_2 , *J. Nucl. Mater.* 377 (2008) 406–408.
- [56] R.J. White, The development of grain-face porosity in irradiated oxide fuel, *J. Nucl. Mater.* 325 (2004) 61–77.
- [57] D. Pizzocri, G. Pastore, T. Barani, A. Magni, L. Luzzi, P.V. Uffelen, S. Pitts, A. Alfonsi, J. Hales, A model describing intra-granular fission gas behaviour in oxide fuel for advanced engineering tools, *J. Nucl. Mater.* 502 (2018) 323–330.
- [58] C.F. Clement, M.H. Wood, *Proc. Roy. Soc. Lond. A* 368 (1979) 521.
- [59] M. Fell, S.M. Murphy, The nucleation and growth of gas bubbles in irradiated metals, *J. Nucl. Mater.* 172 (1990) 1–12.
- [60] F.S. Ham, Theory of diffusion-limited precipitation, *J. Phys. Chem. Solids* 6 (1958) 335–351.
- [61] J. Rest, G.L. Hofman, An alternative explanation for evidence that xenon depletion, pore formation, and grain subdivision begin at different local burnups, *J. Nucl. Mater.* 277 (2000) 231–238.
- [62] D.R. Olander, D. Wongsawaeng, Re-solution of fission gas – a review: Part I. Intragranular bubbles, *J. Nucl. Mater.* 354 (2006) 94–109.
- [63] J. Spino, J. Rest, W. Goll, C. Walker, Matrix swelling rate and cavity volume balance of UO_2 fuels at high burn-up, *J. Nucl. Mater.* 346 (2) (2005) 131–144.
- [64] G. Pastore, D. Pizzocri, C. Rabiti, T. Barani, P. Van Uffelen, L. Luzzi, An effective numerical algorithm for intra-granular fission gas release during non-equilibrium trapping and resolution, *J. Nucl. Mater.* 509 (2018) 687–699.
- [65] M.V. Speight, W. Beere, Vacancy potential and void growth on grain boundaries, *Met. Sci.* 9 (1975) 190–191.
- [66] P. Van Uffelen, Contribution to the Modelling of Fission Gas Release in Light Water Reactor Fuel, Ph.D. thesis, University of Liège, Belgium, 2002.
- [67] D. Pizzocri, F. Cappia, V.V. Rondinella, P. Van Uffelen, Preliminary Model for the Pore Growth in the HBS, Tech. Rep. JRC103064, European Commission, Directorate for Nuclear Safety and Security, JRC-Karlsruhe, 2016.
- [68] G. Pastore, L.P. Swiler, J.D. Hales, S.R. Novascone, D.M. Perez, B.W. Spencer,

- L. Luzzi, P. Van Uffelen, R.L. Williamson, Uncertainty and sensitivity analysis of fission gas behavior in engineering-scale fuel modeling, *J. Nucl. Mater.* 465 (2015) 398–408.
- [69] D.R. Olander, P. Van Uffelen, On the role of grain boundary diffusion in fission gas release, *J. Nucl. Mater.* 288 (2001) 137–147.
- [70] P. Lössönen, On the effect of irradiation-induced resolution in modelling fission gas release in UO_2 LWR fuel, *J. Nucl. Mater.* 496 (2017) 140–156.
- [71] T. Kogai, Modelling of fission gas release and gaseous swelling of light water reactor fuels, *J. Nucl. Mater.* 244 (1997) 131–140.
- [72] M.S. Veshchunov, On the theory of fission gas bubble evolution in irradiated UO_2 fuel, *J. Nucl. Mater.* 277 (2000) 67–81.
- [73] Y. Miao, B. Ye, Z.-G. Mei, D. Andersson, K. Mo, G. Hofman, A.M. Yacout, Fission gas swelling in U_3Si_2 at LWR conditions, in: *Top Fuel 2016*, Boise, Idaho, USA, 2016.
- [74] B. Beeler, M. Baskes, D. Andersson, M.W. Cooper, Y. Zhang, Molecular dynamics investigation of grain boundaries and surfaces in U_3Si_2 , *J. Nucl. Mater.* 514 (2019) 290–298.
- [75] K.A. Gamble, J.D. Hales, G. Pastore, T. Barani, D. Pizzocri, Behavior of U_3Si_2 Fuel and FeCrAl Cladding under Normal Operating and Accident Reactor Conditions, Tech. Rep. INL/EXT-16-40059 Rev. 0, Idaho National Laboratory, 2016, <https://doi.org/10.2172/1364507>.
- [76] C. Vitanza, U. Graziani, N.T. Fordestrømmen, K. Vilpponen, Fission Gas Release from in-pile Measurements, Tech. Rep. HPR-221.10, 1978.
- [77] A. Alfonsi, C. Rabiti, D. Mandelli, J. Cogliati, C. Wang, P.W. Talbot, D.P. Maljovec, C. Smith, RAVEN Theory Manual and User Guide, Tech. Rep. INL/EXT-16-38178, Idaho National Laboratory, 2017.
- [78] C. Rabiti, A. Alfonsi, J. Cogliati, D. Mandelli, R. Kinoshita, S. Sen, C. Wang, J. Chen, RAVEN User Manual, Tech. Rep. INL/EXT-15-34123, Idaho National Laboratory, 2017.